

# Purcell-enhanced single-photon emission from nitrogen-vacancy centers coupled to a tunable microcavity

Hanno Kaupp,<sup>1,2</sup> Thomas Hümmer,<sup>1,2</sup> Matthias Mader,<sup>1,2</sup> Benedikt Schlederer,<sup>1</sup> Julia Benedikter,<sup>1,2</sup> Philip Haeusser,<sup>1</sup> Huan-Cheng Chang,<sup>3</sup> Helmut Fedder,<sup>4</sup> Theodor W. Hänsch,<sup>1,2</sup> and David Hunger<sup>1,2,\*</sup>

<sup>1</sup>*Fakultät für Physik, Ludwig-Maximilians-Universität, Schellingstraße 4, 80799 München, Germany*

<sup>2</sup>*Max-Planck-Institut für Quantenoptik, Hans-Kopfermann-Str. 1, 85748 Garching, Germany*

<sup>3</sup>*Institute of Atomic and Molecular Sciences, Academia Sinica, Taipei 106, Taiwan*

<sup>4</sup>*3. Physikalisches Institut, Universität Stuttgart, Pfaffenwaldring 57, 70569 Stuttgart, Germany*

(Dated: February 16, 2022)

Optical microcavities are a powerful tool to enhance spontaneous emission of individual quantum emitters. However, the broad emission spectra encountered in the solid state at room temperature limit the influence of a cavity, and call for ultra-small mode volume. We demonstrate Purcell-enhanced single photon emission from nitrogen-vacancy (NV) centers in nanodiamonds coupled to a tunable fiber-based microcavity with a mode volume down to  $1.0\lambda^3$ . We record cavity-enhanced fluorescence images and study several single emitters with one cavity. The Purcell effect is evidenced by enhanced fluorescence collection, as well as tunable fluorescence lifetime modification, and we infer an effective Purcell factor of up to 2.0. With numerical simulations, we furthermore show that a novel regime for light confinement can be achieved, where a Fabry-Perot mode is combined with additional mode confinement by the nanocrystal itself. In this regime, effective Purcell factors of up to 11 for NV centers and 63 for silicon vacancy centers are feasible, holding promise for bright single photon sources and efficient spin readout under ambient conditions.

## I. INTRODUCTION

Solid-state-based quantum emitters such as the NV center in diamond are promising for efficient single photon sources [1, 2], quantum memories [3–5], and quantum sensors [6–8], with functionality preserved also under ambient conditions. One of the central challenges is to efficiently access the quantum properties of the emitter by optical means. Free space coupling only achieves low collection efficiency, and poses fundamental limits on achievable fidelities and signal to noise ratios. Optical microcavities [9] allow to enhance the light-matter interaction, and offer an increase in spontaneous emission by the Purcell factor  $C_{\text{eff}} = \frac{3(\lambda/n)^3}{4\pi^2} \frac{Q_{\text{eff}}}{V}$ , together with the potential for near-unity collection efficiency  $\beta = C_{\text{eff}}/(C_{\text{eff}} + 1)$ . Here,  $V$  is the mode volume of the cavity,  $n$  the refractive index, and  $Q_{\text{eff}} = (Q_c^{-1} + Q_{\text{em}}^{-1})^{-1}$  is the effective quality factor combining the quality factor of the cavity ( $Q_c$ ) and of the emitter ( $Q_{\text{em}}$ ) [10, 11]. For broadband emitters such as the NV center,  $Q_{\text{em}}$  as estimated from the linewidth of the emission spectrum is small at room temperature and limits the influence of high  $Q_c$ , and cavities with ultra-small mode volume are required. A lot of effort has been put into realizing coupled systems both with bulk micro- and nanocavities [12–21], as well as tunable open-access microcavities [22–25]. Although cavity-induced lifetime changes have been demonstrated, this has been mostly limited to cryogenic temperatures however, where the zero phonon line is narrow, and the extracted integrated count rates remained well below spectrally integrated free space values. Furthermore, the re-

quired smallest mode volumes have only been achieved in bulk cavities, where limited spectral tunability as well as the difficulty to find or place a single emitter in the cavity field maximum result in low device yield.

Here, we use an open-access tunable microcavity [26–31] with ultra-small mode volume realized by advanced laser machining to demonstrate Purcell-enhanced emission of NV centers in nanodiamonds. We record cavity-enhanced fluorescence images of large areas of the sample by scanning cavity microscopy [27, 31–33] and study several single emitters with one and the same cavity. Photon collection rates from single NV centers of up to  $1.6 \times 10^6 \text{ s}^{-1}$  are observed. Furthermore, we demonstrate continuous spontaneous emission control by varying the mirror separation down to sub- $\mu\text{m}$  mirror separations, where we observe a maximal Purcell factor of 2.0. These results indicate that field confinement by the nanocrystal itself is present in addition to the mode defined by the mirrors. For an optimized geometry, numerical simulations predict an effective Purcell factor of up to 11 for the broad room-temperature emission spectrum of the NV center. At the same time, the outcoupling efficiency from the cavity into a low-NA mode is as high as 51%, limited by the intrinsic loss of the used mirror coating.

## II. ULTRA-SMALL MODE VOLUME TUNABLE CAVITY

The microcavity is assembled of a planar mirror onto which the sample is applied, and a concave mirror on the tip of an optical fiber [26], see Fig. 1(a). The tip of the cavity fiber is shaped by advanced CO<sub>2</sub> laser machining [34, 35]. In a first step, the extent of the end-facet is tapered to enable sub-micron mirror separations,

\* david.hunger@physik.lmu.de

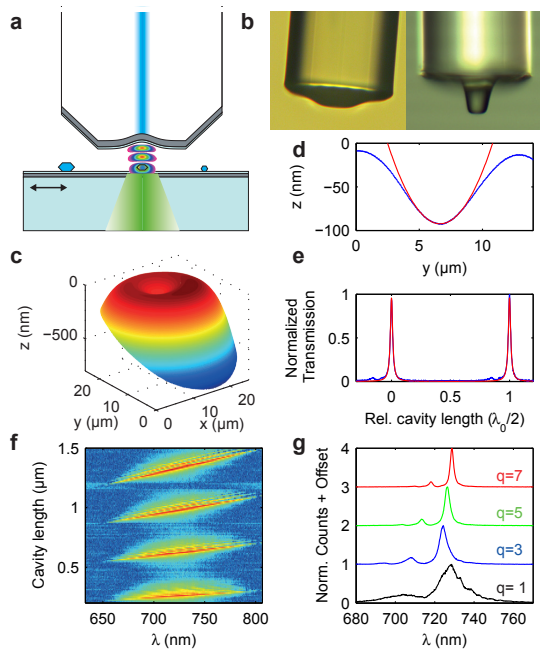


Figure 1. (a) Sketch of the cavity consisting of a laser-machined and mirror-coated fiber and a macroscopic mirror carrying nano diamonds with NV centers. The large mirror is mounted on a three-axis nanopositioning stage for spatial scanning, the cavity length is controlled by an additional piezo actuator. (b) Microscope images (20x) of two laser-shaped fiber tips. (c) 3D profile of a laser-machined and silver-coated fiber tip. (d) Cut through the center of the structure shown in (c) (blue) together with a parabolic fit (red). (e) Cavity transmission probed with a narrow-band laser as a function of the cavity length. (f) Series of cavity transmission spectra under broadband illumination as a function of the cavity length, showing tunability for cavity lengths down to  $\lambda_0/2$ . (g) Individual spectra from (f) for different mode orders  $q$ .

which is crucial when aiming at smallest mode volumes. Therefore, multiple laser pulses are applied in circular patterns to the edge of the endfacet to crop the outer part of the fiber, resulting in a protruding plateau with a diameter of typically below  $20\mu\text{m}$ . Figure 1(b) shows two examples of different shape. Next, a concave depression aligned with the fiber core is produced within the center of the plateau using a few weak laser pulses [36]. To achieve smallest mode volumes, a compromise has to be chosen between the size of the radius of curvature  $r_c$  and the smallest achievable mirror separation, since a small  $r_c$  requires a deep profile. Since we want to study the regime where the diamond crystal provides additional field confinement (see below), we prioritize small mirror separation and compromise on the radius of curvature. Figure 1(c) shows the topography of a machined fiber tip measured with white light interferometry. The central part of the profile is well fitted by a parabola, yielding a radius of curvature  $r_c = 90\mu\text{m}$ , while the full profile fits to a Gaussian with  $1/e$  diameter  $D = 7\mu\text{m}$  and a structure depth  $z < 100\text{nm}$  (Fig. 1(d)).

When choosing an optimal mirror coating, both the mirror reflectivity and field penetration need to be considered. While dielectric coatings provide highest reflectivity and low loss, they exhibit significant field penetration into the coating, which increases the mode volume. Optimizing the Purcell factor for broadband emitters shows that metal coatings with few tens of nm penetration are advantageous, despite the higher loss [31, 37, 38]. We coat the fiber tip with 60nm and the planar mirror with 33nm silver, both finished with a 20nm glass capping to prevent oxidation. This yields reflectivities of 96% and 88% and absorption loss of 4%, while scattering loss is found to be negligible. The two mirrors define an open and tunable plano-concave Fabry-Perot cavity that outcouples up to 51% of the light through the planar mirror into the detection channel (see Appendix). We measure a cavity finesse of  $\mathcal{F} = 42 \pm 1$  at  $\lambda_0 = 690\text{nm}$  by recording the cavity transmission of a narrow-band laser when tuning the cavity length over one free spectral range (Fig. 1(e)).

We determine the mode volume of the cavity by measuring the optical cavity length  $d$  and the mode waist  $w_0$ , and use the expression  $V = \pi w_0^2 d/4$ . To determine  $d$ , we record the cavity transmission under broadband illumination with a spectrometer, see Fig. 1(f,g), and evaluate the separation and location of the resonances. In this way we prove that the shortest resonant cavity length  $d = \lambda_0/2$  is actually reached without touching the planar mirror with the fiber tip, i.e. full tunability is ensured even for the fundamental resonance  $q = 1$ . By scanning the cavity over a point-like object such as a single NV center and collecting the fluorescence emitted into the cavity (Fig. 2(b,c)), the mode waist can be inferred from the observed size of the point spread function  $w_{\text{det}}$  in a cavity-enhanced fluorescence image (see Appendix). We determine a minimal  $w_0 = 1.1\mu\text{m}$  at  $d = \lambda_0/2$ , such that a minimal cavity mode volume  $V = 1.0\lambda_0^3$  ( $0.34\mu\text{m}^3$ ) is achieved.

### III. CAVITY ENHANCED EMISSION FROM SINGLE NV CENTERS

We study a commercial nanodiamond sample (Van-Moppes) with a size distribution between 100 and 200nm, where a reasonable fraction of the crystals contains individual NV centers. The sample is directly spin coated or drop cast onto the planar mirror. As a first step, we record a cavity-enhanced fluorescence image of a large area of the sample by scanning the sample mirror while the cavity length is stabilized to a mirror separation of around  $10\mu\text{m}$ , both the excitation light and the NV emission spectrum being resonant with the cavity (see Appendix). Figure 2(a) shows a scan area of  $(50\mu\text{m})^2$ , where about 50 emitters are visible. The excitation power is 3.6mW at 532nm. The second-order correlation function  $g^{(2)}(\tau)$ , as well as the saturation behavior for the five marked emitters is recorded. A closer

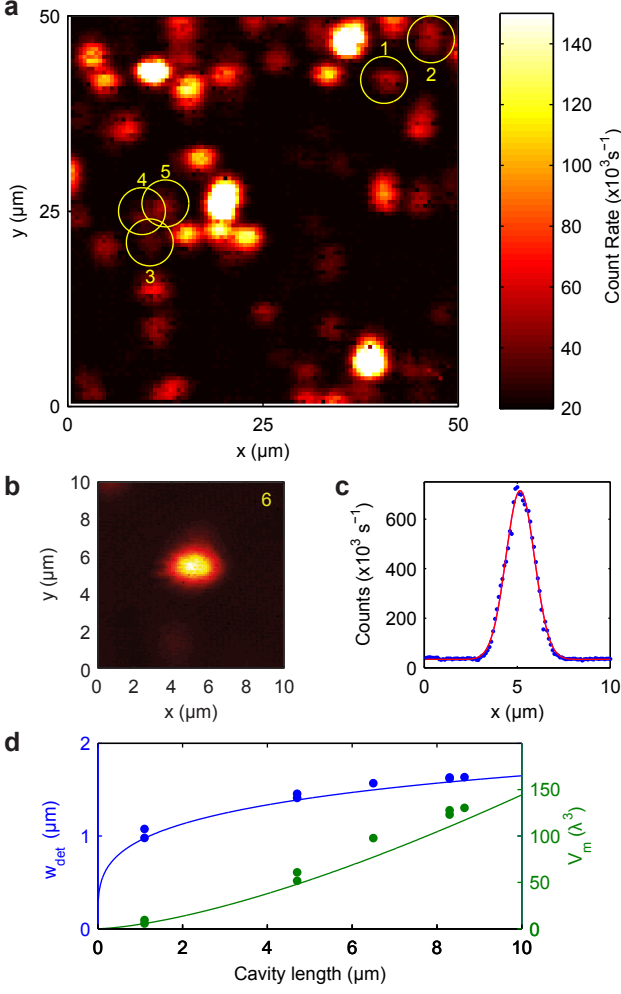


Figure 2. (a) Cavity-enhanced fluorescence image showing several single emitters (circles). The cavity length is stabilized on resonance with the excitation light at a length of about  $10 \mu\text{m}$  while scanned laterally. (b) Cavity scan of a single NV center at  $1.1 \mu\text{m}$  cavity length. (c) Vertical cut through the scan in (b) together with a Gaussian fit, yielding  $w_{\text{det}} = 1.1 \mu\text{m}$ . (d) Measured size of the point spread function (blue points) as a function of the cavity length, together with the value calculated from the radius of curvature of the fiber mirror (blue line). Mode volume calculated from the measured  $w_{\text{det}}$  (green points), together with the expected value (green line).

view on another, more isolated, single NV center (NV6) is shown in Fig. 2(b,c), where the cavity length is stabilized at  $d = 1.1 \mu\text{m}$ . This is the shortest mirror separation, for which the cavity is simultaneously resonant for excitation and fluorescence emission, such that significant Purcell enhancement is present (see below). Since this yields the highest signal to background ratio, we use it for all single-emitter measurements shown here. In the measurement we observe a spatial resolution of  $1.1 \mu\text{m}$ , a high peak count rate ( $K > 6 \cdot 10^5 \text{ s}^{-1}$ ) and a signal-to-background ratio  $> 20$  for the NV center showing clear

antibunching with  $g^{(2)}(0) = 0.21$ . The non-zero values is primarily due to autofluorescence of the mirror coating. With the simultaneous excitation and fluorescence enhancement and the emission into the well-collectable cavity mode, the cavity enables enhanced count rates, and provides spatial and spectral filtering at the same time. Cavity-enhanced scanning fluorescence microscopy thus promises net signal improvement compared to confocal microscopy.

As an example for the single-emitter fluorescence obtainable from the cavity, we discuss the results for one NV center (NV1) in more detail. We measure the  $g^{(2)}$  function at low excitation power and fit it with the function  $g^{(2)}(\tau) = 1 + p(be^{-|\tau|/\tau_2} - (1+b)e^{-|\tau|/\tau_1})$ , which includes antibunching, bunching, and background, see Fig. 3(a). The fit value of  $g^{(2)}(0) = 0.27$  proves that it is a single emitter. Figure 3(b) shows a measurement of the intensity dependent fluorescence rate, which is fitted well by a saturation part and a linear contribution accounting for the background:  $K = K_{\infty}I/(I_{\text{sat}} + I) + aI$  (see Appendix). We find a saturation count rate  $K_{\infty} = 6.9 \cdot 10^5 \text{ s}^{-1}$ , a saturation intensity  $I_{\text{sat}} = 0.49 \cdot 10^9 \text{ Wm}^{-2}$  and a linear background parameter  $a = 100 \cdot 10^3 \text{ s}^{-1}/10^9 \text{ Wm}^{-2}$ . The intensity dependent background count rate is also recorded at a location on the mirror without emitters. The observed slope is equal to the value  $a$  found for the emitter saturation, i.e. the diamond crystal itself does not contribute notable background in this case. The reported count rates are raw values as detected with avalanche photo diodes (APDs). To obtain the number of photons collected by the first lens, we account for the detection efficiency of the optical setup of 43% (see Appendix). From this we find that  $1.6 \times 10^6$  photons per second are collected by the first lens.

To quantify the emission enhancement by the cavity, we study several emitters in the cavity and compare the results with confocal measurements ( $\text{NA}=0.75$ ) of NV centers on a glass substrate. We record the  $g^{(2)}$  function and the saturation count rate of each emitter and compare the results by plotting the saturation count rate versus  $g^{(2)}(0)$  for cavity and free space emission, see Fig. 3(c). Taking background fluorescence into account, we expect all NVs in the cavity with  $g^{(2)}(0) \lesssim 0.7$  being single emitters. The evaluation yields an average detected saturation count rate per NV center of  $K_{\infty} = 5.7 \cdot 10^5 \text{ s}^{-1}$  inside the cavity, in comparison with  $1.5 \cdot 10^5 \text{ s}^{-1}$  on the glass substrate. This corresponds to an average observed enhancement factor of 3.8.

We estimate the theoretically expected enhancement as follows: The photon rate coupled out of the cavity is given by  $K_c = QE \cdot C_{\text{eff}} \gamma \eta_c$ , where  $QE$  denotes the quantum efficiency and  $\gamma$  the excited state decay rate. For the experimental parameters used in the measurements described above, applying the simple Purcell formula, we find  $C_{\text{eff}} \approx 0.12$ , for  $V = 5\lambda^3$ ,  $Q_c = 126$ ,  $Q_{\text{em}} = \frac{\lambda_0}{\Delta\lambda} \approx 8$ , stemming from the center wavelength  $\lambda_0 = 690 \text{ nm}$  and the FWHM  $\Delta\lambda = 90 \text{ nm}$  of the emission spectrum. The

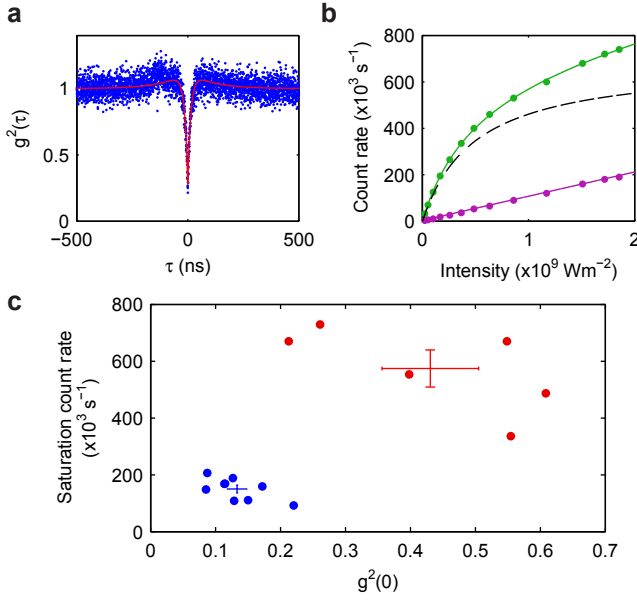


Figure 3. (a) Autocorrelation measurement for NV1 proving single emitter behavior with  $g^{(2)}(0) = 0.27$  without background subtraction. (b) Saturation measurement of the same NV center (green dots) together with a fit (green line). Background fluorescence from the silver mirror (purple dots) together with a linear fit (purple line). NV center fluorescence subtracted by background (black dashed line). (c) Comparison of the saturation count rates and single-photon purities for NV centers on glass (blue dots) and inside the cavity at  $1.1 \mu\text{m}$  cavity length (red dots). An average enhancement by a factor 3.8 is found.

fraction of photons leaving the cavity through the out-coupling mirror is  $\eta_c = 0.51$ , and the cavity mode is fully collected by the objective. For the case of NV centers on a glass substrate, the dipole radiation pattern is affected by the air-glass interface [39, 40]. For the given NA we calculate a collection efficiency of  $\eta_\Omega = 0.16$  and a photon collection rate  $K = QE \cdot \gamma \eta_\Omega$ . The detection efficiency after the objective is assumed to be equal to the cavity case. The total expected enhancement is then  $K_c/K = C_{\text{eff}} \eta_c / \eta_\Omega = 0.4$ , in contrast to the value found in the experiment. This shows that the simplified treatment does not properly describe the situation. In fact, the applied formula is derived in the limit where the cavity mirrors subtend a negligible solid angle and where the dipole remains far from any surface. For a more accurate treatment, we perform analytical [39, 40] and finite difference time domain (FDTD) simulations (Lumerical). We identify three aspects that influence the spontaneous emission beyond the simple treatment: (i) The proximity of the planar mirror surface with the sample leads to self-interference of the dipole radiation over a large angular range as well as to some amount of near-field coupling [39, 40]. A FDTD simulation for an orientation-averaged dipole located in a nanodiamond on a metal mirror predicts a lifetime reduction factor of 1.8

compared to the situation without the mirror, as well as negligible nonradiative decay ( $< 10\%$ ) (see Appendix). (ii) The large solid angle subtended by the cavity mirrors, having an NA close to unity, significantly affects the mode structure beyond the fundamental cavity mode and consequently influences (e.g. inhibits) the decay into modes other than the fundamental cavity mode [41, 42]. (iii) For suitable crystal size and smallest mirror separation, the nanodiamond provides additional lateral mode confinement (see below). All these aspects are captured by FDTD simulations of the emitter inside the cavity, and we obtain an effective Purcell factor of  $C_{\text{eff}} = 1.4$  when comparing the cavity-coupled emission rate with free-space emission. The predicted enhancement is then  $K_c/K = C_{\text{eff}} \eta_c / \eta_\Omega = 4.5$ , about twenty percent larger than determined experimentally. Expected contributions to this deviation are a reduced coupling strength due to non-ideal dipole orientation and a emitter location away from the cavity field maximum.

#### IV. LIFETIME MODIFICATION

A central aspect of the Purcell enhancement is the influence of the cavity on the excited state lifetime. To demonstrate this effect we perform time-correlated single photon counting under pulsed excitation at different mirror separations. In measurements with single emitters we observe significant lifetime variation. However, we find that the lifetime is also affected by varying amounts of background, related to the distance dependent cavity coupling efficiency of the excitation light. To unambiguously demonstrate the effect of the cavity on the lifetime, we therefore study ensembles of NV centers, where background plays a negligible role. We use nanodiamonds with a diameter distribution peaking between 100 and 150 nm that were irradiated with He ions to achieve a high concentration of NV centers ( $\sim 10^2$  per crystal) [43, 44]. In these measurements, the used cavity fiber has a planar endfacet whose edges are mechanically polished off to allow for smallest mirror separations. This simpler geometry stemming from an earlier approach is technically easy to realize and facilitates direct comparison with FDTD simulations. The fiber has an identical coating as in the previous case, while the large mirror has higher transmission due to a thicker glass capping (60 nm), resulting in  $\mathcal{F} = 28$  at 700 nm.

We measure the fluorescence lifetime of the NV center ensemble for different mirror separations by time-correlated single photon counting [45], where we tune the mirror separation with a piezo actuator and calibrate the optical cavity length  $d$  as well as the geometrical mirror separation  $d_0$  from fluorescence spectra [46]. Each decay trace is fitted with a monoexponential decay, from which we obtain the lifetime  $\tau(d_0)$  [47]. Figure 4(a) shows an example measurement. Figure 4(b) presents individual traces for the mirror separations indicated in (a). At the same time, the fluorescence is spec-



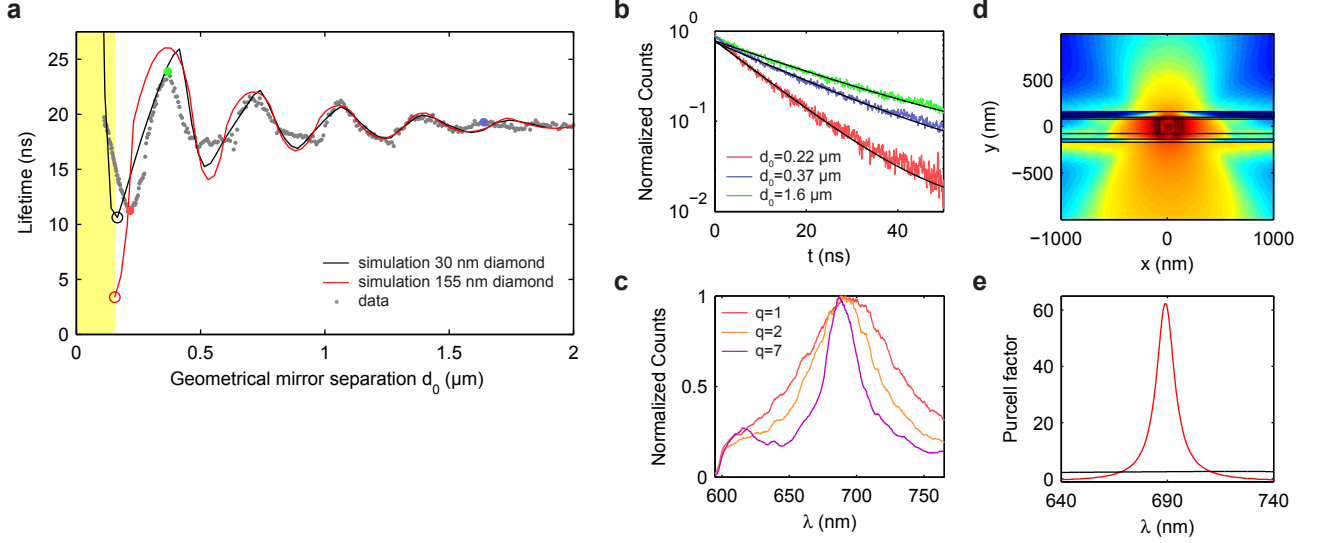


Figure 4. (a) Measured lifetime  $\tau(d_0)$  as a function of the mirror separation (gray dots) together with FDTD simulations for a diamond cube of edge length 30 nm (black line) and 155 nm (red line). The filled colored dots indicate the positions at which the datasets shown in (b) were taken. The yellow area shows the distance range where the fiber touches the large diamond. (b) Lifetime traces for different cavity lengths together with monoexponential fits (black), (red:  $\tau = 11.2$  ns, blue: 19.3 ns, green: 23.9 ns). (c) Cavity emission spectra at resonances corresponding to longitudinal mode orders  $q = 1, 2, 7$ . (d) Simulation of the intensity distribution of a dipole located at the center (logarithmic scale, red: high, blue: low). The intensity is confined between the two silver mirrors (horizontal black lines, including the spacer layers) and localized to the nanocrystal (black square). Outcoupling occurs predominantly through the thinner bottom mirror. (e) Simulated Purcell factor as a function of the wavelength for a 155 nm (red, corresponding to open circle in (a)) and a 30 nm (black) diamond.

trally filtered by the cavity, yielding a resonance with a linewidth depending inversely on the mirror separation, see Fig. 4(c). For cavity lengths below  $2 \mu\text{m}$ , the lifetime is modulated noticeably. Whenever the cavity is resonant (off-resonant) with the emission spectrum, the lifetime is reduced (increased) due to the variation of the local density of states. The shortest (longest) detected lifetime of  $\tau_c = 11.2$  ns (23.7 ns) corresponds to a lifetime reduction (enlargement) of 40 % (25 %) compared to the lifetime of  $\tau_m = 18.9$  ns obtained when the cavity fiber is not present. We estimate the effect of the sample mirror alone from a statistical comparison of lifetimes both on the mirror and on a glass substrate (reduction by a factor of  $1.3 \pm 0.3$ ), as well as from FDTD simulations averaged over dipole orientations (reduction factor 1.8), suggesting a free-space lifetime of up to  $\tau_0 = 34$  ns. With this, we obtain an upper bound for the effective Purcell factor of  $C_{\text{eff}} = \frac{\tau_0}{\tau_c} - 1 = 2.0$ . We have studied several nanocrystals in a similar manner and observe a shortest lifetime of  $\tau_c = 6.7$  ns with comparable relative lifetime changes. At the same time, the integrated fluorescence increases by up to a factor of 40 from  $d = 2 \mu\text{m}$  to  $d = \lambda/2$ . This is due to the fact that the cavity has a negligible effect for large mirror separations and only the emission transmitted through the planar mirror ( $T_1 = 0.11$ ) is collected with a small collection efficiency  $\eta_\Omega = 0.16$ . In contrast, for short cavities, the Purcell effect leads to a dominant emission into the cavity mode, a fraction  $\eta_c = 0.56$  of which is coupled out to the detector side and entirely

collected by the objective (see Appendix).

We compare our results to three dimensional FDTD simulations. The diamond is modeled as a cube with a refractive index of 2.4 and an edge length of 155 nm. In addition, we study a 30 nm crystal for comparison. The individual mirror layers are implemented with parameters as given above. A dipole source peaking at a wavelength of 690 nm with a spectral width of 100 nm is placed at the center of the cube. We perform simulations with a dipole orientation parallel and normal to the plane of the mirrors for different mirror separations. Figure 4(d) shows a cross section of the geometry with a dipole oriented along the  $x$ -axis located in the center. A strong confinement of the intensity to the crystal is visible (note the logarithmic color scale), as well as the directional outcoupling through the bottom mirror. The outcoupled mode has an NA of 0.26 (0.38 after refraction at an air-glass interface), which can be easily collected by an objective. For each cavity length, the simulation evaluates the Purcell factor as a function of the wavelength  $C(\lambda)$ . Figure 4(e) shows an example for the 155 nm crystal at  $d = \lambda/2$ , yielding a peak Purcell factor of  $C = 63$  compared to the nanocrystal in vacuum. To enable a comparison with the experimental data, we normalize  $C(\lambda)$  to the Purcell factor  $C_m(\lambda)$  obtained for simulations where the fiber mirror is removed, and average over the NV emission spectrum  $S(\lambda)$ . The spectrum is modeled as a Gaussian distribution of 110 nm  $1/e$ -full-width, centered at 690 nm. The effective enhancement factor is then determined as

$\tau_c/\tau_m = \int_{-\infty}^{\infty} C(\lambda)C_m(\lambda)^{-1}S(\lambda)d\lambda / \int_{-\infty}^{\infty} S(\lambda)d\lambda$ . The FDTD simulations for the parallel dipole are in good agreement with the measurements. Contributions of the normal dipole component play a negligible role, since this orientation is only weakly excited and coupled to the cavity. For the 155 nm diamond, a maximal effective Purcell factor of  $C_{\text{eff}} = 11$  is predicted when the fiber touches the diamond. In contrast, the 30 nm diamond yields a much smaller Purcell factor, and the enhancement spectrum  $C(\lambda)$  does not show a clear resonance (see Fig. 4(e)).

## V. WAVEGUIDE EFFECT

We explain the large Purcell factor by additional mode confinement of suitably sized nanocrystals. Some intuition about the confinement effect can be drawn from modeling the crystal as a cylindrical waveguide [48] with refractive index  $n_d = 2.4$  and solving the Helmholtz equation for the electric field  $(\nabla^2 + k^2)E = 0$  in one dimension. Here,  $k = 2\pi n_r/\lambda$ , with  $n_r = n_d$  for  $|r| \leq b$  and 1 for  $|r| > b$ ,  $r$  is the transverse coordinate, and  $b$  the waveguide radius. We find that the propagating waveguide mode shows strongest confinement around  $b = 70$  nm, yielding a minimal effective mode radius  $(1/e^2)$  of  $w_0 = 160$  nm. A segment of such a nanowire can now be considered to be introduced into a planar Fabry-Perot cavity with mirror separation  $d = \lambda/2n_{\text{eff}}$ , where  $n_{\text{eff}}$  is the effective refractive index experienced by the propagating mode (we find  $n_{\text{eff}} = 1.88$  for  $b = 70$  nm). The mode volume of such a cavity would amount to  $V = \pi w_0^2 \lambda / 8n_{\text{eff}} = 0.07 (\lambda/n_{\text{eff}})^3$ , substantially smaller than what is achievable by conventional curved-mirror Fabry-Perot cavities. Together with an effective quality factor  $Q_{\text{eff}} = 8$ , this yields  $C_{\text{eff}} = 8$ , in reasonable agreement with the FDTD simulation. From the more reliable FDTD simulations we find an optimal crystal size around 155 nm for a cubic shape. A  $\pm 10\%$  size variation does not significantly affect the maximal  $C$ , while the enhancement rapidly diminishes for crystals  $< 140$  nm and no additional enhancement is obtained for the 30 nm crystal.

The measurement also suggests the presence of a contribution of the waveguide effect. Experimental imperfections, averaging over dipole orientation, and finite quantum efficiency are expected to lead to a reduced lifetime modification. This is evident most clearly e.g. at the lifetime minima corresponding to the resonances  $q = 2$  and  $q = 3$ , where the lifetime reduction in the data remains smaller than in the simulation for both crystal sizes [49]. However, for  $q = 1$ , where the waveguide effect is expected to be present, the experimental variation is as large as the simulated ideal variation for the 30 nm crystal. Consequently, the Purcell factor in the experiment needs to be larger than in the simulation to compensate for the imperfections. The increase of the measured lifetime towards smallest  $d$  indicates a crystal size below 140 nm, which could in part explain the smaller effect.

## VI. CONCLUSION

We have demonstrated that improved laser machining enables the realization of stable Fabry-Perot cavities with mode volumes down to  $1 \lambda^3$ , while maintaining full tunability. Multiple emitters can be investigated with a single cavity, and efficient single photon extraction is possible even for broadband emitters. The Purcell enhancement together with high outcoupling efficiency allows net count rates exceeding free-space collection. Furthermore, we have shown with simulations that suitably chosen nanodiamonds can provide exceptional mode confinement. Predicted ideal Purcell factors up to 63 could be fully exploited with narrow-band emitters such as the SiV center in diamond, and effective Purcell factors for NV centers up to 11 are expected. While our experiments already indicate a contribution due to this effect, we expect that more controllably fabricated diamond nanostructures [8, 50, 51] can unfold the full potential of this approach and pave the way for ultra-bright single photon sources and superior readout of single spins under ambient conditions.

## ACKNOWLEDGEMENTS

We thank Aniket Agrawal and Tolga Bagci for contributions to the experiment, as well as Philipp Altpeter for assistance in the cleanroom. Fruitful discussions with Christoph Becher, Jason Smith, and Jörg Wrachtrup are acknowledged. The work has been funded by the European Union 7th framework Program under grant agreement no. 61807 (www.fp7wasps.org) and the DFG Cluster of Excellence NIM. T. W. Hänsch acknowledges funding from the Max-Planck Foundation.

## APPENDIX A: CAVITY CHARACTERIZATION AND SETUP

*Mirror coating* The fiber tips are coated with a 60 nm silver film and finished with a 20 nm glass capping to prevent oxidation. Consistent with simulations [52] we measure a reflectivity of  $R_2 = (92 \pm 2)\%$  at 532 nm. The macroscopic planar mirror is prepared on a low autofluorescence glass substrate with a 33 nm thick silver layer and an analogous glass capping. At a wavelength of 532 nm we measure a mirror transmission of  $T_1 = 15\%$ . A simulation yields the transmission and absorption loss of the two mirrors at 700 nm:  $T_1 = 8\%$ ,  $T_2 = 0.8\%$  and  $A_1 = 4\%$ ,  $A_2 = 3\%$ . With atomic force microscopy measurements we determine the surface roughness of the silver mirrors to be  $< 5$  nm rms, such that scattering loss plays a negligible role ( $< 0.5\%$ ). The measured finesse agrees well with the transmission and loss values, and we calculate the expected fraction of photons leaving the cavity through the macroscopic mirror to be  $\eta_c = T_1/(T_1 + T_2 + A_1 + A_2) = 0.51$ . Despite the lossy

character of the metal coatings, a high outcoupling efficiency is achieved. For the plane-plane cavity, the glass capping layer of the macroscopic mirror is increased to 60 nm, resulting in an increased transmission,  $T_1 = 24\%$  at 532 nm and 11% at 700 nm, respectively. The outcoupling efficiency amounts to  $\eta_c = 0.56$  at 700 nm.

*Mode volume* The mode volume of a plano-concave cavity is given by  $V = \pi w_0^2 d / 4$ , with the mode waist  $w_0^2 = \lambda / \pi \cdot \sqrt{r_c d - d^2}$  and the optical cavity length  $d = \frac{\lambda}{2} \left[ q + \frac{\zeta}{\pi} \right] \approx q \frac{\lambda}{2}$  for  $r_c \gg d$ . Here,  $q$  is the longitudinal mode order, and  $\zeta = \arccos \sqrt{1 - d/r_c}$  is the Gouy phase. The finite conductivity of the silver mirror and the capping layer leads to some field penetration into the mirror, such that the geometrical mirror separation  $d_0 = \frac{\lambda}{2} \left[ q + \frac{\zeta - \phi}{\pi} \right]$  is smaller than  $d$ . This is accounted for by the average deviation of the reflection phase from  $\pi$ ,  $\phi = \pi - (\phi_1 + \phi_2)/2$ . At  $\lambda = 700$  nm,  $\phi_1 \approx \phi_2 = 0.72\pi$  for our mirrors [53], and we calculate an air gap of  $d_0 = 260$  nm for  $q = 1$ . This value reduces further when a nanodiamond of significant size is placed in the cavity mode due to the effective refractive index change.

*Point spread function* In cavity-enhanced fluorescence scans, the observed point spread function is the product of the cavity mode for emission ( $w_0$ ) and excitation ( $w_e = \sqrt{\lambda_e / \lambda} w_0$ ). The size of the point spread function is then  $w_{\text{det}} = w_e w_0 / \sqrt{w_e^2 + w_0^2}$ , which can be used to determine  $w_0$ . The experimental values agree well with a calculation for different cavity lengths when using the measured radius of curvature of the fiber mirror, see (Fig. 2(d)).

*Setup* The cavity is embedded into a confocal microscope setup, similar to the one described in [23]. Excitation is performed with either a cw laser at 532 nm or a band-pass filtered supercontinuum source ( $\sim 50$  ps pulse length, 20 MHz repetition rate) through a cover slip

corrected microscope objective (NA=0.75) through the planar mirror. Alternatively, the excitation can be performed through the cavity fiber. For pulsed excitation we use average excitation powers ranging from a couple of ten to a few hundred  $\mu\text{W}$ . The planar mirror is mounted on a three-axis slip-stick nanopositioner allowing to scan the mirror for suitable emitters. The fiber is mounted on a stacked piezo actuator which allows for precise tuning and stabilization of the cavity length. The latter is performed by using the green excitation light transmitted through the cavity to generate a cavity length-dependent feedback signal, which is fed to the stacked piezo controlling the fiber position.

*Excitation intensity* For the saturation measurements and autocorrelation measurements of single emitters in the cavity (Fig. 3) we excite through the cavity fiber with 532 nm light. We calculate the excitation intensity  $I$  inside the cavity from the measured transmitted power  $P_t$ , the outcoupling mirror transmission  $T_1$ , and the evaluated excitation mode waist  $w_e$  according to  $I = \frac{8P_t}{\pi w_e^2 T_1}$ .

*Detection efficiency* We infer the detection efficiency of the setup by coupling a laser at 690 nm into the cavity fiber with the cavity on resonance and measure the transmission of the mode coupled out of the cavity through the optics up to the APDs. A fraction of 67% of the light reaches the detectors at a cavity length of 1  $\mu\text{m}$ . Together with the quantum efficiency of the APDs of 65%, a detection efficiency of 43% at 690 nm is achieved.

*Nonradiative decay* To study the onset of nonradiative decay, we simulated the quantum efficiency of a dipole in a diamond cube (edge length 30 nm) on a silver mirror (layer thickness 33 nm) with an intermediate glass spacer layer of variable thickness. For glass layers larger than 30 nm, the quantum efficiency exceeds 90% for dipoles parallel to the mirror surface. Since the applied spacer layers have a thickness of 60 nm, we expect the amount of nonradiative decay to be less than 10%.

- 
- [1] C. Kurtsiefer, S. Mayer, P. Zarda, and H. Weinfurter, *Physical Review Letters* **85**, 290 (2000).
  - [2] I. Aharonovich, S. Castelletto, D. A. Simpson, C.-H. Su, A. D. Greentree, and S. Prawer, *Reports on Progress in Physics* **74**, 076501 (2011).
  - [3] P. Neumann, R. Kolesov, B. Naydenov, J. Beck, F. Rempp, M. Steiner, V. Jacques, G. Balasubramanian, M. L. Markham, D. J. Twitchen, J. Pezzagna, S. and Meijer, J. Twamley, F. Jelezko, and J. Wrachtrup, *Nature Physics* **6**, 249 (2010).
  - [4] G. D. Fuchs, G. Burkard, P. V. Klimov, and D. D. Awschalom, *Nature Physics* **7**, 789 (2011).
  - [5] P. C. Maurer, G. Kucsko, C. Latta, L. Jiang, N. Y. Yao, S. D. Bennett, F. Pastawski, D. Hunger, N. Chisholm, M. Markham, and et al., *Science* **336**, 1283 (2012).
  - [6] G. Balasubramanian, I. Y. Chan, R. Kolesov, M. Al-Hmoud, J. Tisler, C. Shin, C. Kim, A. Wojcik, P. R. Hemmer, A. Krueger, T. Hanke, A. Leitenstorfer, R. Bratschkitsch, F. Jelezko, and J. Wrachtrup, *Nature* **455**, 648 (2008).
  - [7] J. R. Maze, P. L. Stanwix, J. S. Hodges, S. Hong, J. M. Taylor, P. Cappellaro, L. Jiang, M. V. G. Dutt, E. Togan, A. S. Zibrov, A. Yacoby, R. L. Walsworth, and M. Lukin, *Nature* **455**, 644 (2008).
  - [8] P. Maletinsky, S. Hong, M. S. Grinolds, B. Hausmann, M. D. Lukin, R. L. Walsworth, M. Loncar, and A. Yacoby, *Nature Nanotechnology* **7**, 320 (2012).
  - [9] K. J. Vahala, *Nature* **424**, 839 (2003).
  - [10] A. Auffeves, D. Gerace, J.-M. Gerard, M. F. Santos, L. C. Andreani, and J.-P. Poizat, *Physical Review B* **81**, 245419 (2010).
  - [11] A. Meldrum, P. Bianucci, and F. Marsiglio, *Optics Express* **18**, 10230 (2010).
  - [12] J. Wolters, A. W. Schell, G. Kewes, N. Nüsse, M. Schöngen, H. Döschner, T. Hannappel, B. Löchel, M. Barth, and O. Benson, *Applied Physics Letters* **97**, 141108 (2010).

- (2010).
- [13] D. Englund, B. Shields, K. Rivoire, F. Hatami, J. Vucovic, H. Park, and M. D. Lukin, *Nano Lett.* **10**, 3922 (2010).
  - [14] P. E. Barclay, K.-M. C. Fu, C. Santori, A. Faraon, and R. G. Beausoleil, *Physical Review X* **1**, 011007 (2011).
  - [15] A. Faraon, P. E. Barclay, C. Santori, K.-M. C. Fu, and R. G. Beausoleil, *Nature Photon* **5**, 301 (2011).
  - [16] T. van der Sar, J. Hagemeyer, W. Pfaff, E. C. Heeres, S. M. Thon, H. Kim, P. M. Petroff, T. H. Oosterkamp, D. Bouwmeester, and R. Hanson, *Applied Physics Letters* **98**, 193103 (2011).
  - [17] B. J. M. Hausmann, B. J. Shields, Q. Quan, Y. Chu, N. P. de Leon, R. Evans, M. J. Burek, A. S. Zibrov, M. Markham, D. J. Twitchen, and et al., *Nano Lett.* **13**, 5791 (2013).
  - [18] J. C. Lee, D. O. Bracher, S. Cui, K. Ohno, C. A. McLellan, X. Zhang, P. Andrich, B. Aleman, K. J. Russell, A. P. Magyar, and et al., *Applied Physics Letters* **105**, 261101 (2014).
  - [19] L. Li, T. Schröder, E. H. Chen, M. Walsh, I. Bayn, J. Goldstein, O. Gaathon, M. E. Trusheim, M. Lu, J. Mower, and et al., *Nat Comms* **6**, 6173 (2015).
  - [20] J. Riedrich-Möller, S. Pezzagna, J. Meijer, C. Pauly, F. Mücklich, M. Markham, A. M. Edmonds, and C. Becher, *Applied Physics Letters* **106**, 221103 (2015).
  - [21] T. Schröder, S. L. Mouradian, J. Zheng, M. E. Trusheim, M. Walsh, E. H. Chen, L. Li, I. Bayn, and D. Englund, *J. Opt. Soc. Am. B* **33**, B65 (2016).
  - [22] R. Albrecht, A. Bommer, C. Deutsch, J. Reichel, and C. Becher, *Physical Review Letters* **110** (2013), 10.1103/physrevlett.110.243602.
  - [23] H. Kaupp, C. Deutsch, H.-C. Chang, J. Reichel, T. W. Hänsch, and D. Hunger, *Physical Review A* **88** (2013), 10.1103/physreva.88.053812.
  - [24] R. Albrecht, A. Bommer, C. Pauly, F. Mücklich, A. W. Schell, P. Engel, T. Schröder, O. Benson, J. Reichel, and C. Becher, *Applied Physics Letters* **105**, 073113 (2014).
  - [25] S. Johnson, P. R. Dolan, T. Grange, A. A. P. Trichet, G. Hornecker, Y. C. Chen, L. Weng, G. M. Hughes, A. A. R. Watt, A. Auffeves, and J. M. Smith, *New J. Phys.* **17**, 122003 (2015).
  - [26] D. Hunger, T. Steinmetz, Y. Colombe, C. Deutsch, T. W. Hänsch, and J. Reichel, *New J. Phys.* **12**, 065038 (2010).
  - [27] C. Toninelli, Y. Delley, T. Stöferle, A. Renn, S. Götzinger, and V. Sandoghdar, *Applied Physics Letters* **97**, 021107 (2010).
  - [28] P. R. Dolan, G. M. Hughes, F. Grazioso, B. R. Patton, and J. M. Smith, *Opt. Lett.* **35**, 3556 (2010).
  - [29] M. Trupke, E. A. Hinds, S. Eriksson, E. A. Curtis, Z. Moktadir, E. Kukharenska, and M. Kraft, *Applied Physics Letters* **87**, 211106 (2005).
  - [30] R. J. Barbour, P. A. Dalgarno, A. Curran, K. M. Nowak, H. J. Baker, D. R. Hall, N. G. Stoltz, P. M. Petroff, and R. J. Warburton, *Journal of Applied Physics* **110**, 053107 (2011).
  - [31] H. Kelkar, D. Wang, D. Martin-Cano, B. Hoffmann, S. Christiansen, S. Götzinger, and V. Sandoghdar, *Physical Review Applied* **4**, 054010 (2015).
  - [32] M. Mader, J. Reichel, T. W. Hänsch, and D. Hunger, *Nat Comms* **6**, 7249 (2015).
  - [33] L. Greuter, S. Starosielec, D. Najer, A. Ludwig, L. Duempelmann, D. Rohner, and R. J. Warburton, *Applied Physics Letters* **105**, 121105 (2014).
  - [34] D. Hunger, C. Deutsch, R. J. Barbour, R. J. Warburton, and J. Reichel, *AIP Advances* **2**, 012119 (2012).
  - [35] K. Ott, S. Garcia, R. Kohlhaas, K. Schüppert, P. Rosenbusch, R. Long, and J. Reichel, arXiv:1603.04791 (2016), 1603.04791.
  - [36] For some geometries it is advantageous to create the concave profile before tip shaping.
  - [37] M. Steiner, F. Schleifenbaum, C. Stupperich, A. Failla, A. Hartschuh, and A. Meixner, *Journal of Luminescence* **119-120**, 167 (2006).
  - [38] M. Steiner, A. Hartschuh, R. Korlacki, and A. J. Meixner, *Applied Physics Letters* **90**, 183122 (2007).
  - [39] W. Lukosz and R. Kunz, *JOSA* **67**, 1607 (1977).
  - [40] W. Lukosz, *JOSA* **69**, 1495 (1979).
  - [41] G. Meurant, *Advances in Atomic, Molecular, and Optical Physics*, Advances In Atomic, Molecular, and Optical Physics No. Bd. 28 (Elsevier Science, 1991).
  - [42] Z. Di, H. V. Jones, P. R. Dolan, S. M. Fairclough, M. B. Wincott, J. Fill, G. M. Hughes, and J. M. Smith, *New J. Phys.* **14**, 103048 (2012).
  - [43] N. Mohan, Y.-K. Tzeng, L. Yang, Y.-Y. Chen, Y. Y. Hui, C.-Y. Fang, and H.-C. Chang, *Advanced Materials* **22**, 843 (2010).
  - [44] S.-J. Yu, M.-W. Kang, H.-C. Chang, K.-M. Chen, and Y.-C. Yu, *Journal of the American Chemical Society* **127**, 17604 (2005).
  - [45] A. I. Chizhik, A. M. Chizhik, D. Khoptyar, S. Bär, A. J. Meixner, and J. Enderlein, *Nano Lett.* **11**, 1700 (2011).
  - [46] In the measurement shown in Fig. 4(e), we observe a deviation of the actual cavity length from the expected value below  $d \sim 500$  nm, most probably due to the cavity fiber touching the large mirror with one of its edges. We have adjusted the distance calibration below 500 nm to restrict the cavity lengths to  $d > 100$  nm.
  - [47] We note that in general, a multi-exponential decay is expected due to the position and dipole orientation distribution of the colour centers in the nanodiamond. Fitting the data with stretched exponentials [54] yields a larger lifetime modulation, such that the evaluation shown is a conservative estimate.
  - [48] T. M. Babinec, B. J. M. Hausmann, M. Khan, Y. Zhang, J. R. Maze, P. R. Hemmer, and M. Loncar, *Nature Nanotechnology* **5**, 195 (2010).
  - [49] We note that a small amount of parasitic lifetime modulation seems to be also present, again most probably due to the varying amount of excitation light coupled into the cavity and the corresponding variation of background contribution. It can be seen at large mirror separation (e.g. for  $d > 1.3 \mu\text{m}$ ) with a periodicity of 270 nm.
  - [50] C. Arend, P. Appel, J. N. Becker, M. Schmidt, M. Fischer, S. Gsell, M. Schreck, C. Becher, P. Maletinsky, and E. Neu, *Applied Physics Letters* **108**, 063111 (2016).
  - [51] S. A. Momenzadeh, R. J. Stöhr, F. F. de Oliveira, A. Brunner, A. Denisenko, S. Yang, F. Reinhard, and J. Wrachtrup, *Nano Lett.* **15**, 165 (2015).
  - [52] S. A. Furman and A. V. Tikhonravov, *Basics of Optics of Multilayer Systems* (World Scientific Publishing, 1992).
  - [53] H. Becker, S. E. Burns, N. Tessler, and R. H. Friend, *Journal of Applied Physics* **81**, 2825 (1997).
  - [54] M. N. Berberan-Santos, E. N. Bodunov, and B. Valeur, *Chemical Physics* **315**, 171 (2005).